Grain Boundary Defect Chemistry of Acceptor-Doped Titanates: High Field Effects

MARKUS VOLLMANN & RAINER WASER

Institut für Werkstoffe der Elektrotechnik, RWTH Aachen, 52056 Aachen, Federal Republic of Germany

Abstract. The field enhanced average conductivity in grain boundary space charge depletion layers in acceptor-doped $SrTiO_3$ ceramics was investigated by impedance analysis in the time domain. The dependence of the grain boundary conductivity on the acceptor concentration, the temperature and the field dependence are discussed and interpreted in terms of a Schottky diffusion model combined with the influence of accumulated oxygen vacancies at the GB interface.

I. Introduction

Charge transport across grain boundaries is a well known subject of investigation for a variety of ceramic materials which exhibit ionic conduction, electronic conduction or mixed ionic-electronic conduction. In a broad range of these materials the grain boundary acts as a barrier for the cross-transport of charge carriers. In perovskite-type titanates, the barrier character is especially pronounced in the low temperature regime which is the common working regime of high permittivity dielectrics such as acceptor-doped titanates used for multi-layer capacitors (MLCs). Due to the continuous trend of miniaturization for these devices and for unaltered operating voltages the dielectric is subjected to higher field stresses. For instance, an applied operating voltage of 15 V at a capacitor with an inner thickness of 5 μm leads to a field stress of 3 MV/m. Under these high fields the grain boundary conductivity exhibits a field enhanced current across the barrier leading to a reduced life-time due to the effect of resistance degradation. This component related problem is the motivation for a closer look at the grain boundary (GB) barriers in acceptor doped titanates.

The residual low-field conductivity within the grain boundaries (width: up to 100 nm) of typical acceptor-doped alkaline-earth titanate ceramics was found to be below 10^{-11} S/m in the operating temperature regime of MLC components ($T < 400$ K) [1]. As described in detail in our preceding papers [1,2], the GB barrier is usually caused by positively charged, donor type GB states oppositely charged compared to the acceptor dopant centers in the bulk. This causes a depletion of the mobile carriers such as oxygen vacancies and holes in the vicinity of the grain boundary. These GB depletion space charge layers are described as back-to-back double Schottky barriers.

In the present paper, we report on the *conductivity* in the GB space charge layer, σ_{GB}, and its dependence on the *electric field strength*. The influence of a broad variety of external and material parameters will be discussed. It will be pointed out that σ_{GB} is an *averaged* conductivity across the space charge layer. We have restricted our study to the low temperature regime ($T < 650$ K) in which no equilibration with the oxygen partial pressure of the ambient atmospheres takes place within reasonable measuring times due to the slow kinetics of the oxygen exchange reaction via the sample surfaces [3,4].

In section II, we describe the sample preparation and the measuring techniques. An overview of our recent results for the low-field GB conductivity will

be given in section III. A general survey of possible mechanism of known nonlinearity effects for the electrical conductivity is outlined in section IV(1). Experimental data of the high field GB conductivity are presented in section IV(2). A Schottky diffusion model for the GB characteristics in acceptor-doped SrTiO$_3$ ceramics is introduced and detailed in the following section (section IV(3)). The dependence on the temperature, the acceptor concentration and especially the field dependence of the GB conductivity are discussed and interpreted in section IV(4)–(5).

With respect to the future development of MLCs towards higher capacitance-to-volume ratios especially by decreasing the dielectric thickness between the inner electrodes, two essential aspects of the conductivity in the GB space charge region, σ_{GB}, have to be considered:

(1) It is known that the *insulation resistance* of titanate ceramic components decreases reversibly under electrical fields exceeding a critical value [21]. This critical value is well below the break down strength, E_{BD}, under which the irreversible destruction of the component takes place. As will be confirmed and elaborated in this paper, the reversible field-stimulated enhancement of the conductivity is obviously restricted to the GB space charge region.

(2) The *life time* of components based on acceptor doped titanate dielectrics under dc field stress is limited by the long term resistance degradation (see [6] and references cited therein) caused by a re-distribution of the oxygen vacancies between the electrodes. The ionic portion within the conductivity σ_{GB} determines the kinetics of this degradation [21]. The ionic and the electronic contributions to the field enhanced charge transport across GB barriers will be identified in the present paper.

II. Experimental

The same acceptor-doped SrTiO$_3$ ceramic samples were used as in the experiments of the preceding paper [2]. Discs of 125 μm, 250 μm, and 500 μm thickness were cut, lapped and polished and electrodes of NiCr alloy and Au were applied by evaporation.

We have used the voltage step technique, described in our preceding paper [2], covering a voltage range from 1–1000 V and a temperature range from 390–650 K. After every voltage step measurement, at a certain temperature and before applying an increased voltage, the sample is refreshed with a voltage cycle. To remove a possible accumulation of oxygen vacancies at the GB barrier due to the measurement, we apply the same but reverse voltage for the measurement time to the sample.

Figure 1 shows the results of dc voltage step experiments at 573 K and different field strengths E for 0.2 at% Ni-doped SrTiO$_3$.

According to the brick-wall model used in Ref. [2], the ceramic can be described by an equivalent network consisting of a bulk branch (B) and a grain boundary branch (GB), each branch represented by an average capacitance ($C_{GB} \gg C_B$) and resistance ($R_{GB} \gg R_B$), i.e., the equivalent circuit means two parallel R–C circuits in series.

The log-log scale in the *time-domain diagram* of Fig. 1 reveals two conductivity values, the short-term conductivity $\sigma_s := \sigma(t \rightarrow 0)$ and the long-term conductivity $\sigma_l := \sigma(t \rightarrow \infty)$. The short-term conductivity σ_s is approximately equal to the bulk conductivity σ_B provided the average grain size d_{gr} is much larger than the GB space charge layer width d_{GB} and provided the charge transport along the grain boundaries is small compared to the charge transport in the grains, which applies to our ceramics. After the completion of the Maxwell–Wagner polarization (i.e., in terms of the network model, the large capacitance C_{GB} is completely charged through the small resistance R_B and $R_{tot} = R_{GB} + R_B$) the leakage current is determined by the total long-time resistance of the ceramic disc. As pointed out in our preceding paper [1], the GB conductivity can be obtained from the plot in Fig. 1 as follows:

$$\sigma_{GB} = \frac{\sigma_l \cdot \sigma_B}{\sigma_B \cdot \dfrac{d_{gr}}{D_{GB}} - \sigma_l \cdot \dfrac{d_{gr} - d_{GB}}{d_{GB}}} \qquad (1)$$

This equation is independent of the electrode area A and the thickness d_{tot} of the sample disc as required. The relation $d_{gr} \gg d_{GB}$ remains valid in all our samples independent of the field-strength leading to

$$\sigma_{GB} = \frac{d_{GB}}{d_{gr}} \cdot \frac{\sigma_l \cdot \sigma_B}{\sigma_B - \sigma_l} \qquad (2)$$

In the low-field case and for most high field cases, $\sigma_l \ll \sigma_s$, as revealed by Fig. 1. Applying this fact
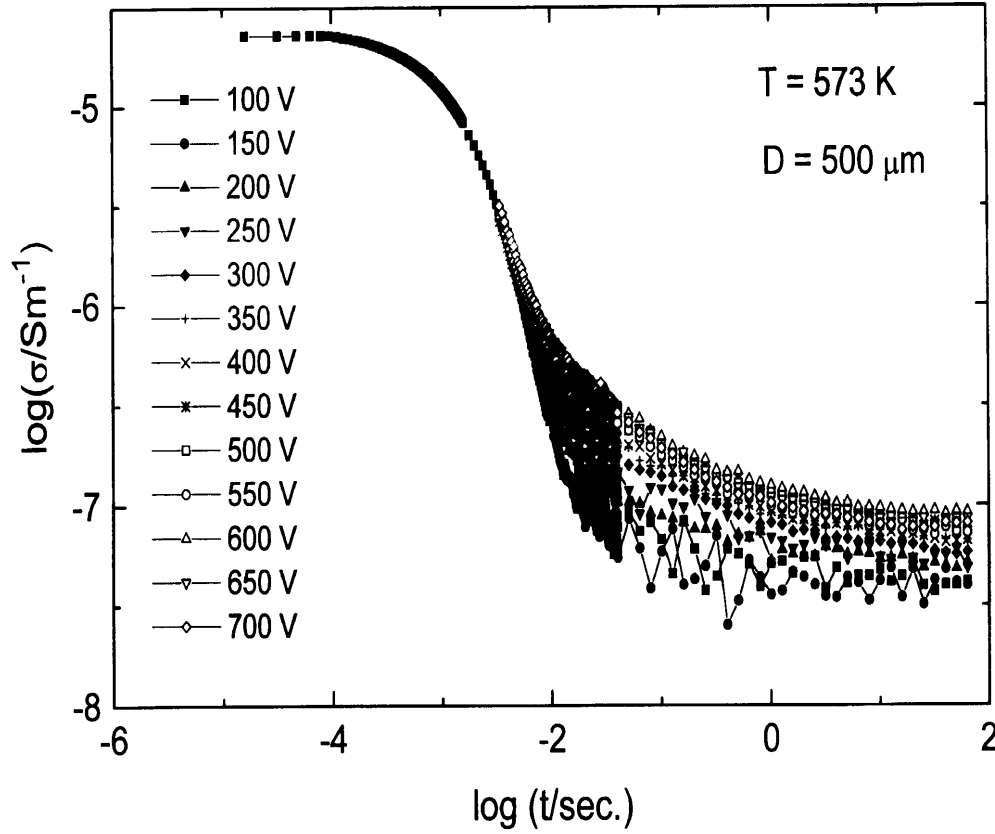
Fig. 1. Illustration of the dc voltage step measurement ($|J/E|$ vs. time on a log-log scale) of 0.2 at% Ni-doped SrTiO$_3$ at $T = 573$ K at different applied voltages. The samples were annealed at Po$_2^{Eq} = 10^5$ Pa at 973 K.

together with $\sigma_B \approx \sigma_s$ Eq. (2) results in the approximation

$$\frac{\sigma_{GB}}{\sigma_l} \approx \frac{d_{GB}}{d_{gr}} \qquad (3)$$

As unequivocally demonstrated by Fig. 1, the short-term conductivity σ_s and, hence, the bulk conductivity $\sigma_B \approx \sigma_s$ is completely independent of the external field strength E. The Maxwell–Wagner relaxation time τ given by

$$\tau = R_B \cdot C_{GB} \qquad (4)$$

is obtained from the plots of the time-domain measurements at times clearly before the field enhanced splitting of the curves occurs. Hence, the space charge layer width d_{GB} is almost field independent as long as the occupation of the charged interface states is not affected by the external field [10]. The voltage independence of the Maxwell–

Wagner relaxation time τ implies a voltage independent capacitance C_{GB}. A voltage dependence of C_{GB} would arise from the GB interface charge Q_{GB} as a function of voltage and, hence, as a precondition, partially filled interface states. Our measurements obviously show no field-dependence of C_{GB}, which leads to the assumption that the interface states are completely filled. The field dependence of the long-term conductivity σ_l, in accordance with the Eq. (3), shows in good approximation the field dependence of the GB conductivity σ_{GB}, as discussed in section IV.

III. Low Field GB Conductivity

In this section, we describe the main properties of the ohmic, low field GB conductivity as described in detail in our recent paper [1].
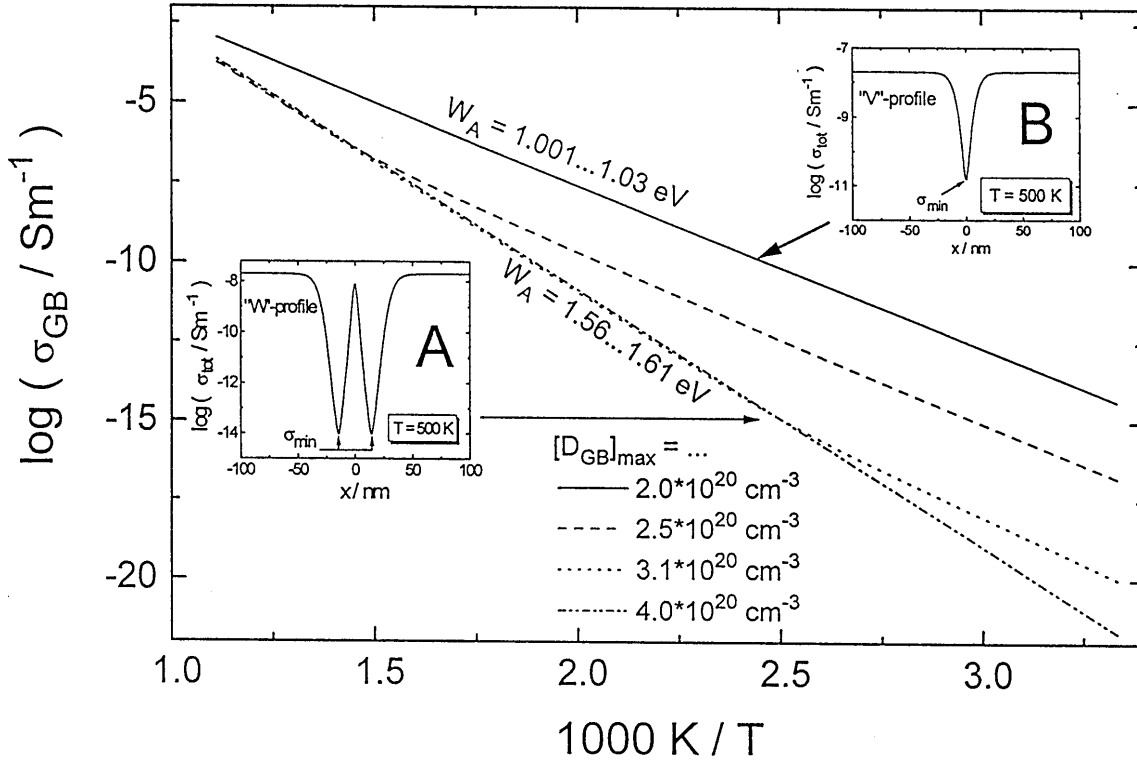
Fig. 2. Simulation of the temperature dependence of the GB-conductivity of 0.1 at% Ni-doped SrTiO$_3$ [1] with different concentrations of the charged donors at the GB-interface [D'_{GB}]. The low slope results from a ''V''-profile of σ_{tot} (low [D'_{GB}], inset B) of $\sigma_{GB}(x)$ and the high slope is determined by a ''W''-profile of σ_{tot} (high [D'_{GB}], inset A).

The most important feature to be emphasized is that the effective GB conductivity is determined by two different profiles of the local conductivity across the GB space charge region, depending on the temperature. At low temperatures, a so called V-type profile dominates, built up by the hole concentration which decays within the grain boundary region with a steep slope in a logarithmic scale. The average GB conductivity is determined here by the minimum conductivity σ_{min} (see inset B in Fig. 2). The GB barrier will increase in this V-type region linearly with temperature due to the validity of Curie–Weiss law for the dielectric constant ε_r (see Eq. (9)). At higher temperatures, the effective positive charge of the interface states will be reduced by electrons, whose concentration rises within the grain boundary due to the law of mass action $n \cdot p = k(T)$. This effect stabilizes the GB barrier at 1.8 eV and decreases slowly with increasing temperature. If the concentration of electrons becomes larger than the hole concentration, the V-type profile of the GB

conductivity is succeeded by a so called W-type profile [1,27]. Both conductivity profiles are time independent (i.e., in thermodynamic equilibration) and the profiles are sketched in the insets of Fig. 2. The temperature dependence of the GB conductivity within the temperature range where the V-type profile is applicable, is given by an activation energy equal to the difference between the Fermi level and the valence band due to the dominating hole conductivity at the grain boundary. The average GB conductivity for the W-type conductivity profile, where the inversion of electrons takes place, is determined by the two conductivity minima σ_{min} (see inset A in Fig. 2) which occur at positions, where the electron conductivity equals the hole conductivity with $\sigma_n = \sigma_p$. Hence, the activation energy for the temperature dependence of the W-type profile GB conductivity is determined by half the band gap energy of SrTiO$_3$ ($W_g = 1.6$ eV).

The simulation shown in Fig. 2 fits the experimental results well and also explains the dependence

of the GB conductivity on acceptor concentration and oxygen partial pressure during equilibration.

IV.   Results and Discussion

(1)   Charge Transport across Barriers: Known Phenomena

In this section, we discuss phenomena which lead to a field dependent electrical conductivity with applicability to dielectric ceramics.

Tunneling effects take place at a potential barrier, whose width is clearly below 10 nm. Tunneling is a well known effect in SiO_2 based materials used as modified MOSFETs for non-volatile memory devices [10]. Emission of charge carriers across the potential barrier by the temperature-independent *Fowler–Nordheim tunneling* takes places if the tip of a potential barrier is sufficiently narrow (< 5 nm) and energetically high. It is a temperature independent process which has been observed at $Au/Si_3N_4/Si$ and $Au/SiO_2/Si$ contacts [10]. The band structure and the temperature dependence do not suggest Fowler–Nordheim tunneling to be significant at grain boundaries in our titanate ceramics. Due to the essentially temperature independence of the Fowler–Nordheim tunneling, it dominates only at temperatures far below room temperature and is succeeded at higher temperatures by other temperature activated and field enhanced current effects.

Such an effect is *Poole–Frenkel emission* due to field enhanced thermal excitation of trapped electrons into the conduction band, i.e., by a local increase of the carrier concentration within the bulk due to de-trapped electrons. In acceptor-doped titanates the deep acceptor levels are approximately 1 eV above the top of the valence band (bandgap energy of $SrTiO_3$ approx. 3.3 eV). Decreasing the potential barrier by e.g., 0.05 eV, an electric field strength of $E_{GB}^{ext} = 10^7 - 10^8$ V/m acts on the depletion layer according to the formula [10,11]:

$$\Delta\Phi = \sqrt{\frac{qE_{GB}^{ext}}{\pi\varepsilon_0\varepsilon_{GB}}} \qquad (5)$$

The nonlinear behavior of σ_{GB} in acceptor doped $SrTiO_3$ begins already at fields of approximately $E_{GB}^{ext} = 10^7$ V/m [7], hence the Poole–Frenkel effect must be considered for our samples.

The Poole–Frenkel effect is a bulk effect and is well known when describing insulating layers such as Si_3N_4 isolating metal electrodes (Au) from semi-conducting materials (Si) for diode purposes. The resulting nonlinear conductivity can be described in terms of the field enhanced lowering of the trap barrier Φ_{trap} on the order of $\Delta\Phi$ (see Eq. (5)):

$$\sigma_{GB} = \sigma_{sat}(T) \cdot \exp\left(-q\frac{\Phi_{trap} - \Delta\Phi}{kT}\right) \qquad (6)$$

where σ_{sat} is the undisturbed conductivity without traps. If $\Delta\Phi$ is equal to the trap depth Φ_{trap}, no charge carriers will be trapped and the nonlinear behavior of the GB conductivity reaches the saturation value. For our samples, the saturation value for $q\Delta\Phi$ obtained from Eq. (5) is about 30 meV using a saturation field strength of $5 \cdot 10^7$ V/m as obtained from our measurements. A simulation using Eq. (6) shows a good fit only with a trap energy of $q \cdot \Phi_{trap} = 80$ meV and a higher field strength than the calculated averaged E_{GB} (one order of magnitude). This trap depth is very small and cannot be explained in terms of trapped holes by charged acceptors, which are known to be about 1 eV above the valence band. Such a small energy of 80 meV is only observed for the oxidation enthalpy to *form* trapped holes by equilibration of the ceramic with a given oxygen partial pressure during annealing [8]. This shallow trap energy can be applicable for oxygen vacancies trapped at negatively charged acceptors. This effect can play a certain role due to the fact, that not all oxygen vacancies contribute to the dominant ionic conductivity as predicted by the vacancy compensation [5] and hence by the acceptor concentration. A possible explanation is the trapping of these oxygen vacancies by charged acceptors. Sufficiently high field stresses which can be found within the depletion zone can release these charge carriers in terms of the Poole–Frenkel effect.

At the electrode interface in electroytes, a strong dependence of the discharge rate of ions on an external applied voltage drop, which differs from the equilibrium potential drop, is observed. This phenomenon is described by the *Butler–Volmer equation* [12] considering a linear varying electrical potential within a small sheet (one atomic-layer) built up by the solvated ions near the electrodes superimposing the Gibbs activation energy for charge transfer to the electrode. A similar effect describing the thermal activated charge transport over an extended potential

barrier in solids is known as Schottky emission. In this model the thermionic emission current depends strongly on the applied field as pointed out in section III(3).

A refined Schottky emission model was used by Pike and Seager [15] to explain the super-ohmic behavior of common polycrystalline semiconductors such as Si. In these materials, the energy distribution of the densities of interface states N_{GB} was found to affect the voltage ΔV_{GB} at which the enhancement of the conductivity sets in. The mean free path l of the charge carriers in semiconducting Si is larger than d_{GB}, hence the transport across grain boundaries is due to the thermionic emission (real Schottky emission). In our dielectric SrTiO$_3$ samples the mean free path of the oxygen vacancies and the holes are in the order of the lattice parameter, i.e., they are much smaller than the GB space charge layer width leading to a hopping of the electronic carriers in accordance with a diffusion model which must be considered.

The electronic charge transport in acceptor doped SrTiO$_3$ must be described in terms of polaron hopping [16]. Despite this, polarons show under sufficient high field stress a strong *decreasing* of their mobility [17].

Although the grain boundary conductivity σ_{GB} rises under high field stresses, it clearly remains below the bulk conductivity σ_B (see Fig. 1) as long as resistance degradation does not set in, resulting in a virtual field free bulk not affected by increasing field strengths.

Integration of the total charge profile, i.e., the space charge and the GB charge $\rho(x) = \rho_A(x) + e_0 N_{GB}(x)$ with $\rho_A(x)$, the space charge concentration caused by the ionized acceptors and $N_{GB}(x)$, the charged interface concentration, leads to the following *b*uild-*in* field profile obtained from the Poisson equation without application of an external field:

$$E^{bi}(x) = \frac{1}{\varepsilon_0 \varepsilon_{GB}} \int_{-d_{GB}^-}^{+d_{GB}^+} \rho(x) dx$$

$$= E_A(x) + E_{GB}(x) \qquad (7)$$

where E_A represents the contribution due to the space charge profile $\rho_A(x)$ and E_{GB} the contribution due to the charge Q_{GB} in the GB plane. Without an external applied field $d_{GB}^- = d_{GB}^+ = d_{GB}/2$ (see Eq. (17)) is valid.

Without applying an external field, the slope of $E^{bi}(x)$ causes a symmetrical band bending downwards as described in [2]. For a 0.1 at% Ni-doped SrTiO$_3$

ceramic a maximum local field-strength at the grain boundary (*without* an external applied field) $E_{max}^{bi} = E_{GB}^{bi}(x = 0)$ of approx. $2 \cdot 10^7$ V/m is obtained from the measured data.

In Fig. 3, σ_{GB} is shown as a function of the *external* field $E = U/D$, where U is the applied voltage and D denotes the overall sample thickness, measured at different temperatures. Due to the fact that $R_B \ll R_{GB}$, nearly the whole field strength is concentrated in the grain boundary region and the bulk can be regarded as virtually field free. The field strength at the grain boundary E_{GB}^{ext} resulting from the external applied field E^{ext} (without local, intrinsic field) can be obtained from the following equation as a formal average value:

$$\text{averaged field:} \quad E_{GB}^{ext} = \frac{d_{gr}}{d_{GB}} \cdot E^{ext}$$

$$= \frac{d_{gr}}{D \cdot d_{GB}} \cdot V \qquad (8)$$

where d_{gr} denotes the average grain size, which is in the range of 2–22 μm for our sample series (see Table 1 in Ref. [2]). With an average GB depletion layer width d_{GB} of about 100 nm the field strength at the grain boundary E_{GB}^{ext} is about 1–2 orders of magnitude higher than the external applied field strength E^{ext}.

The average electrical field stress $E = V/D$ is included as an additional abscissa to E_{GB}^{ext} in Fig. 3. The average voltage drop per grain boundary as calculated by $\Delta V_{GB} = (d_{gr}/D) \cdot V$ can also be obtained from dividing the externally applied voltage by the average number of grain boundaries between the electrodes. At a low voltage drop, i.e., the field across a GB depletion layer $E_{GB}^{ext} = V_{GB}/d_{GB} \ll E_{max}^{bi}$, σ_{GB} exhibits an ohmic behavior. If E_{GB}^{ext} reaches the order of magnitude of E_{max}^{bi}, σ_{GB} starts to enhance strongly with increased voltage. This field enhanced conductivity regime is succeeded at very high fields by a slightly sub-ohmic regime. An investigation towards even higher fields is limited by the resistance degradation. While the time constant τ of the Maxwell–Wagner polarization turned out to be field independent as described above, the time onset of resistance degradation, τ_{RD}, is shifted to shorter times with increasing field, $\tau_{RD} \sim E^{-n}$ with $n = 1.5 \dots 2.5$ [6]. When τ_{RD} is in the same order of magnitude as τ or even below, σ_{GB} can no longer be detected.
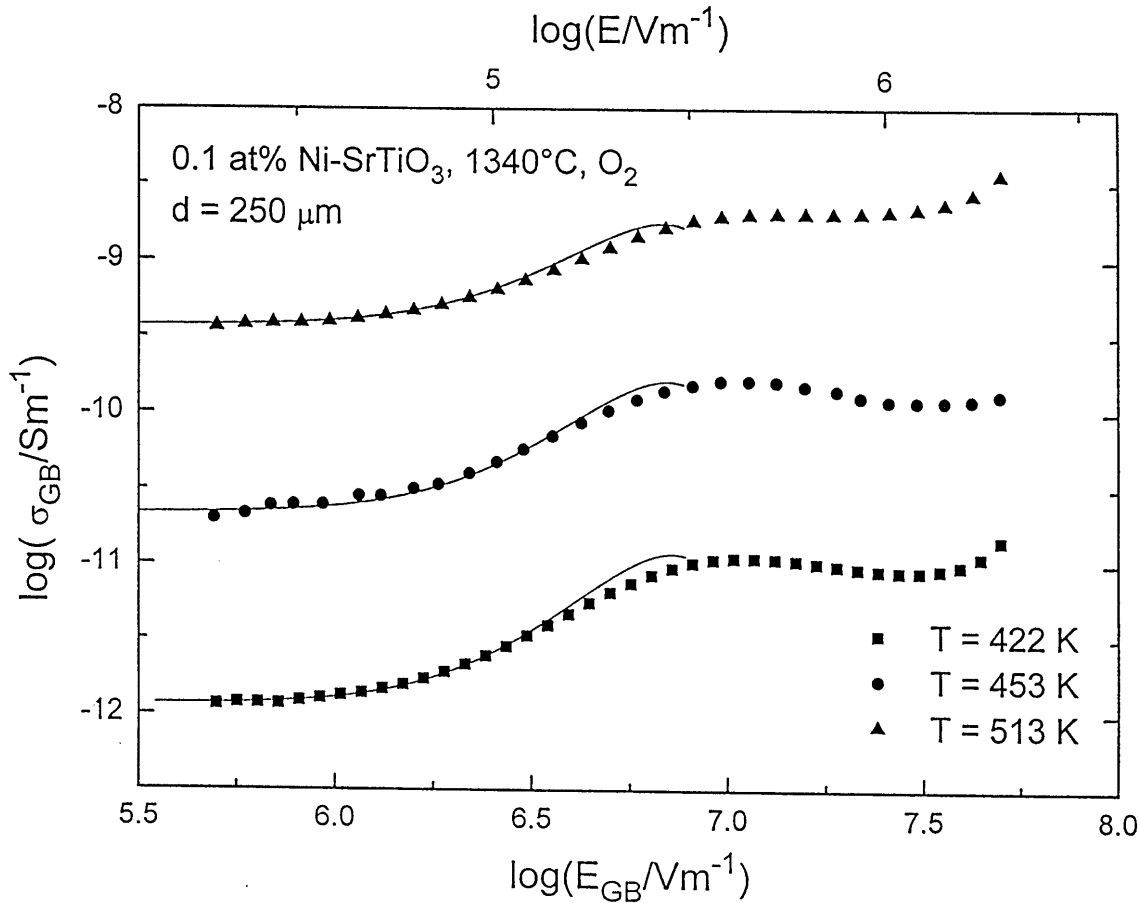
Fig. 3. Field dependence (external applied field $E = V/D$, where D denotes the overall sample thickness) of the GB-conductivity σ_{GB} for 0.1 at% Ni-doped SrTiO₃ measured at different temperatures ($T = 422\,K$ (■), $T = 453\,K$ (●) and $T = 513\,K$ (▲)) and $t = 300\,s$. Solid curves: numerical results obtained from Eq. (14). At high fields the resistance degradation can be seen.

(2) Nature of the GB Conductivity in Acceptor doped SrTiO₃

Evidence supporting the predominant electronic nature of σ_{GB} is given by the concentration profile of the mobile charges in the depletion layer. As revealed in [2], the oxygen vacancy concentration decays in much steeper fashion from the bulk into the depletion layer than the corresponding hole concentration profile. The double positive charge of the oxygen vacancies results in an electrical repulsive force due to the positive charged interface states which is twice the force acting on the single positively charged holes.

In Fig. 3, the nonlinear range can be characterized by a nonlinearity coefficient $\alpha := d(\log I)/d(\log V)$. The ohmic range in the low field regime ($\alpha = 1$) is followed by the super-ohmic range with α-values of approximately 2. This is clearly below the *n*-conducting ZnO-Varistors having α-values of 50 and higher [13]. Increasing the voltage V_{GB} the varistor regime is followed by a subohmic regime in which the maximum value of σ_{GB} does not reach the value of the bulk conductivity, in contrast to semiconducting ZnO varistors. This suggests that the potential barrier has not completely vanished. The experimentally determined, averaged low field GB conductivity σ_{GB} is 3–4 orders of magnitude below the bulk conductivity and the high field GB conductivity in the high field ohmic regime σ_{GB}^{hf}, is 2–3 orders of magnitude lower than the

bulk conductivity. Hence the barrier of the grain boundary is still there and only somewhat decreased. This fact is an important key towards finding an explanation for the field enhancement of the GB conductivity in acceptor doped SrTiO$_3$.

Since the ohmic regime of σ_{GB} in the low field case is supposed to be predominantly electronic, the varistor-like behavior under high field stresses can be explained by the Schottky diffusion model for the current which will be outlined in the following section.

(3) The Schottky Diffusion Model

For our model of the space charge depletion region we have made the following simplifying approximations [2]: (1) a depletion region with a box type profile, (2) a plane two-dimensional interface with charge $Q_{GB}^{\square}$, and (3) a spatially homogeneous acceptor concentration. The barrier height Φ_{GB} is a function of the voltage drop V_{GB}. For one acceptor type with an energy level ΔW_A above the valence band W_V one obtains [13,15]:

$$\Phi_{GB}(V_{GB}) = \Phi_{GB}(V_{GB} = 0)\left(1 - \frac{V_{GB}}{4\Phi_{GB}}\right)^2$$

with   (9)

$$\Phi_{GB} = \frac{Q_{GB}^{\square_2}}{8\varepsilon_0\varepsilon_{GB}e[A']}$$

The interface states are assumed to be treated as narrow energetically distributed, shallow donor states. Due to the acceptor doping, the Fermi level is around the acceptor level (2 eV below the conduction band), hence the interface states must be regarded as completely unoccupied.

Equation (9) depends strongly on the positive interface charge $Q_{GB}^{\square}$ which seems to be independent of the voltage drop over the barrier for Ni-doped SrTiO$_3$ and, hence, the quasi Fermi level will not reach the shallow interface donor levels in the field enhanced GB conductivity regime. The diffusion theory by Schottky described in Ref. [10] is derived from the following assumptions that (1) the built-in barrier height is much larger than kT, which is valid for our temperature range (400–650 K), (2) the effect of hole collision within the depletion region is included, (3) the hole concentrations at $x = -d_{GB}/2$ and $x = +d_{GB}/2$ are unaffected by the current flow (i.e., they have their equilibrium values), and (4) the impurity concentration of the conducting ceramic is

nondegenerate. Since the current in the space charge depletion region depends on the local field and the concentration gradient, the following equation for the current density takes place:

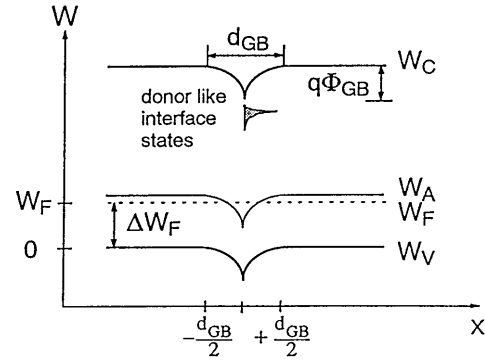$$j_{tot} = q\left[p(x)\cdot\mu_p\cdot E(x) + D_p\frac{\partial p}{\partial x}\right] \quad (10a)$$

with

$$j_{tot} \approx j_p \gg j_{V_{\ddot{o}}}(V\text{-profile}) \quad (10b)$$

where $q = 1.6\cdot10^{-19}$ C and D_p and μ_p are the hole diffusion constant and hole mobility, respectively. Using the Nernst–Einstein relation one obtains from Eq. (10a):

$$j_{tot} = qD_p\left[-\frac{qp(x)}{kT}\frac{\partial\Phi(x)}{\partial x} + \frac{\partial p}{\partial x}\right] \quad (11)$$
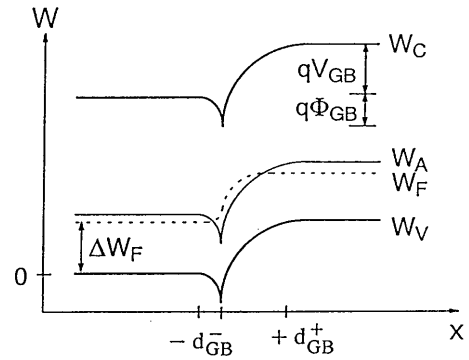

Fig. 4. (a) Plot of the band-bending without bias calculated by defect chemical calculation at $T = 500$ K. (b) Sketch of the influence of a voltage drop V_{GB} across the grain boundary.

Applying the boundary conditions for acceptor doped SrTiO$_3$ for the left (anode) and the right (cathode) side of the grain boundary (see Fig. 4b)

$$q\Phi\left(x = -\frac{d_{GB}}{2}\right) = -\Delta W_F \qquad (12a)$$

and

$$q\Phi\left(x = +\frac{d_{GB}}{2}\right) = -\Delta W_F - qV_{GB} \quad (12b)$$

and

$$p\left(x = -\frac{d_{GB}}{2}\right) = p\left(x = +\frac{d_{GB}}{2}\right)$$

$$= N_v \cdot \exp\left(\frac{-\Delta W_F}{kT}\right) \quad (13)$$

with ΔW_F as the difference between the Fermi level W_F in the bulk and the top of the valence band W_V (see Fig. 4a) and N_V as the density of states at the valence-band. Together with the expression of the band bending for samples without bias

$$q\Phi(x) = -q\phi_{GB}\left(1 - \frac{2|x|}{d_{GB}}\right)^2 \text{ for } |x| \leq d_{GB}/2 \quad (14)$$

one obtains a term for the Schottky diffusion current over a double Schottky barrier in accordance to Ref. [13]:

$$j_{schottky} = j_{SD}\left[1 - \exp\left(\frac{-qV_{GB}}{kT}\right)\right] \quad (15)$$

with V_{GB} as the voltage drop across the grain boundary (see Fig. 4b) and the saturation current density j_{SD}:

$$j_{SD} = \left[\frac{q^2 D_p N_V}{kT}\left[\frac{q \cdot [A']}{\varepsilon_{GB}} \cdot \varepsilon_0 \cdot d_{GB}(V_{GB})\right]\right.$$

$$\left. \cdot \exp\left(\frac{-q\Phi_{GB}(V) - \Delta W_F}{kT}\right)\right] \quad (16)$$

Equation (15) is valid in general for a current across a double Schottky barrier as known from ZnO-varistors, but Eq. (16) is only applicable for our acceptor-doped SrTiO$_3$ due to the special boundary conditions in Eqs. (12)–(14). The voltage dependent GB depletion width is given by:

$$d_{GB}^-(U_{GB}) = d_{GB}^+(U_{GB}) + \frac{2\varepsilon_0\varepsilon_{GB}}{Q_{GB}} \cdot |U_{GB}| \quad (17)$$

$$d_{GB}^+(U_{GB}) = \frac{Q_{GB}}{2q[A']}\left(\frac{1 - |U_{GB}|}{4\Phi_{GB}}\right) \quad (18)$$

with

$$d_{GB} = d_{GB}^+(U_{GB}) + d_{GB}^-(U_{GB}) \neq f(U_{GB}) \quad (19)$$

Equations (17) and (18) are known from metal-semiconductor contacts [10] and describe the voltage dependent depletion width in the semiconductor. For our material, Eq. (17) shows a slight increase of the depletion region on the cathode side and Eq. (18) a decrease on the anode side due to hole conduction. Equations (15)–(19) are only valid for $U_{GB} < \phi_{GB}(U_{GB})$. The total sum of both sides ($= d_{GB}$) is voltage independent for low and medium field stresses due to the electroneutrality conditions, which are still valid.

Equation (15) shows, in the small signal regime, an ohmic behavior ($qV_{GB} \gg kT$) of σ_{GB} followed by a nonlinear characteristic which finally leads to a saturation of the current at sufficiently high fields which is not equivalent to a vanishing of the barrier. The critical field strength $E_{crit} \approx 10^7$ V/m, where the nonlinearity for our samples starts, has the same order of magnitude as calculated from Eq. (16) and the nonlinearity part fits well with the measured curve (see lines in Fig. 3).

Nevertheless, we must take into consideration that Eq. (16) is only applicable as long as the expression $\Phi_{GB} - U_{GB} \geq 0$ is fulfilled. $\Phi_{GB} - U_{GB} = 0$ is equivalent to a flatband condition when σ_{GB} becomes equal to σ_B. This is obviously not observed in our acceptor doped titanates.

Equation (16) is only valid for the temperature range up to 700 K, where the V-type GB conductivity profile is applicable (see our recent paper [1]). The inversion of the electron concentration within the depletion zone resulting in a W-type GB conductivity profile includes an additional degree of complexity in Eq. (16) which changes the behavior of the barrier height Φ_{GB} in Eq. (9) where Q_{GB} must be replaced by the effective positive charge at the interface

$$Q_{GB}^{eff} = Q_{GB}^{\square} - n(x = 0) \cdot dx \quad (20)$$

with n as the electron concentration within the grain

boundary (for $n(x)$ see medium of the W-profile in Fig. 2, inset A). In Eq. (16), a V-type profile is assumed due to the structure of the band bending and the equation contains no information about a concentration enhancement of minority charge carriers such as electrons.

If we take a closer look at the field-enhanced long term conductivity in the time domain where the saturation regime appears and the barrier Φ_{GB} is lowered (Fig. 3) and two differences in the voltage step measurements compared to the low and medium field regime are seen, where a pronounced Maxwell–Wagner relaxation is obvious. The relaxation time τ is changed to slightly lower values meaning a decrease of the GB capacitance $C_{GB} = \tau_R/R_B$. The small decrease of the GB capacitance implies a slight rise of the amount of Q_{GB} and hence an increasing of the barrier height Φ_{GB}. A possible explanation can be seen in Fig. 6a, where the field dependence of the depletion region on the anodic side d_{GB}^{+} and the barrier

height (Fig. 6b) is simulated. In the small and middle field region, the depletion region on the anodic side is nearly voltage independent. At a certain field strength, falling together with the second high-field plateau, the depletion zone shows a rapid shrinkage. At this field strength the barrier height is not vanished (see Fig. 6b) and acts further on as a barrier for the oxygen vacancies. This accumulation of oxygen vacancies within the small depletion zone on the anodic side (several nm) leading to an increasing of the barrier, itself supressing the Schottky diffusion current of holes over the barrier. This mechanism can explain the selfstabilizing of the barrier.

We must remember, that the charge accumulation at the grain boundary is not completed before a new voltage is applied to the sample due to the refresh cycle mentioned in section II. Hence, a possible resistance degradation described in detail in Ref. [6] is prevented which is obviously seen in the unchanged short term conductivity at the higher voltage.
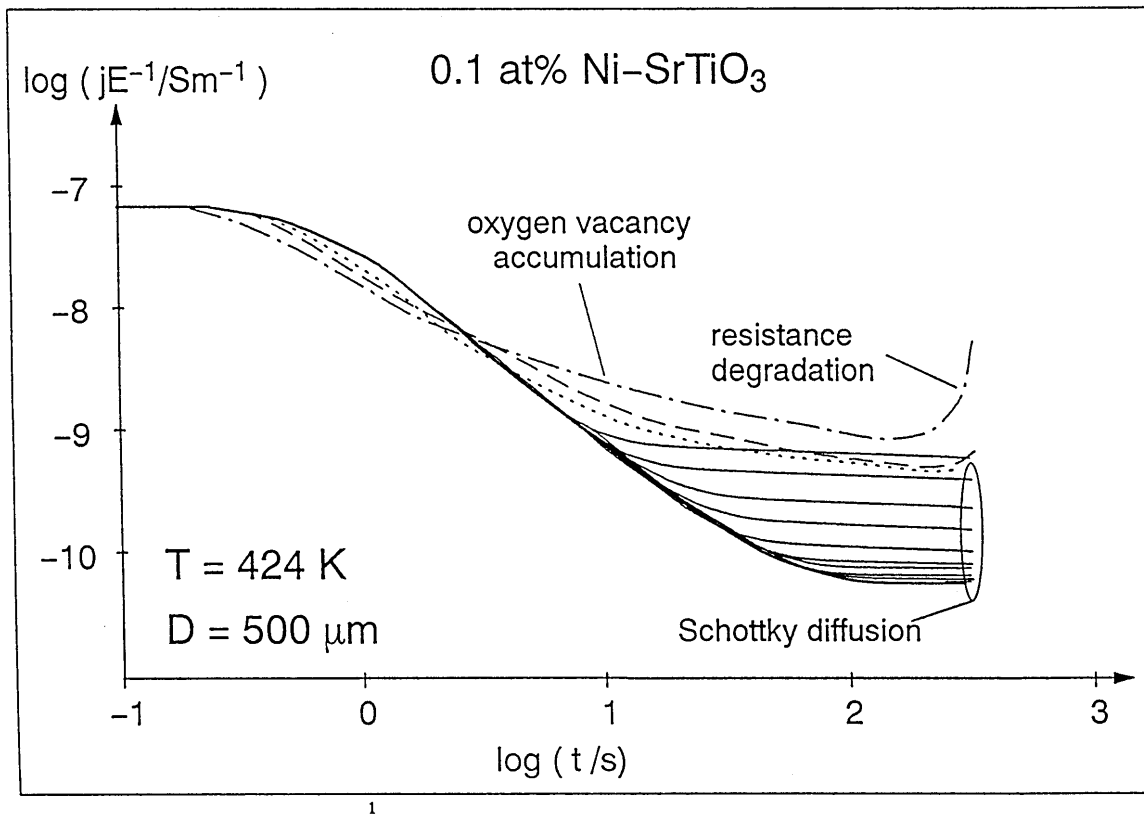

Fig. 5. A more detailed examination of the voltage step measurement results for 0.2 at% Ni-SrTiO₃ at $T = 424$ K. Focus on the semi-saturation regime at sufficiently high field stresses.

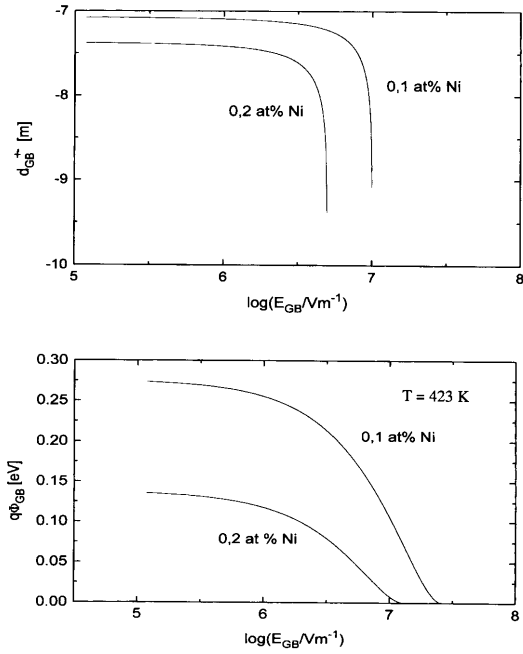*Fig. 6.* Simulation of the (a) voltage dependence of anode sided d_{GB}^+ and (b) field dependence of the barrier Φ_{GB} for different Ni-acceptor concentrations at $T = 423\,$K. The barrier profile is only valid as long as the value for d_{GB}^+ does not vanish. If the d_{GB}^+ value becomes below 1 nm, the barrier stabilization due to oxygen vacancies must be considered.

In Fig. 3 and Fig. 5 it can be seen, that the resistance degradation influences the GB-conductivity at slightly higher field stresses after the pinning or decreasing of the barrier has appeared. This is clear because an accumulation of oxygen vacancies leads to a new defect chemistry equilibrium enhancing the electronic charge carrier concentration [6]. Hence, the occurrence of the semi-saturated, field enhanced GB conductivity is a symptom of the resistance degradation, which starts at slightly higher field stresses and is also an important indication that the accumulation theory is applicable.

(4) Effect of Temperature

The temperature dependence of the low-field conductivity is dominated in Eq. (16) by the exponential term:

$$j_{SD} \propto \exp\left(\frac{-q\Phi_{GB}(V)}{kT}\right) \cdot \exp\left(\frac{-\Delta W_F}{kT}\right)$$

$$(21)$$

The GB barrier height is temperature dependent due to the Curie–Weiss behavior of the dielectric constant ε_r:

$$\varepsilon_{GB} = \frac{C}{T - T_c} \quad \text{with} \quad C = 78,000\,\text{K}$$

$$\text{and} \quad T_c = 27\,\text{K} \qquad (22)$$

Inserting Eq. (22) in Eq. (21) and Eq. (9) leads to a low field GB conductivity (at external applied $V = 1\,$V), dominated by the exponential term which contains the barrier height. This decreases only one order of magnitude with increasing temperature from 400 K to 1000 K. The experimental results show a low field σ_{GB} which increases several orders of magnitude in this temperature range with an activation energy of about 1 eV at lower temperatures (room temperature—650 K). This can be clearly explained by the second exponential term containing the height of the Fermi level (see Fig. 4a).

This is in good agreement with our recent paper, where the thermal activation of the low field conductivity is determined by the minimum conductivity σ_{min} represented by a V-type conductivity profile in the depletion region. The temperature dependence of this minimum is clearly *p*-type which depends on the acceptor-level and the height of the Fermi level, respectively. Defect chemical calculations show, that the Fermi level is 0.1–0.2 eV below the acceptor level and depends on the position of the acceptor level. The following levels are assumed for our bulk acceptors: For Ni′ 0.15 eV, Ni″ 1.2 eV, for Fe′ 0.9 eV and for Mn′ 1.5 eV [1,26].

In Fig. 3, σ_{GB} is plotted as a function of the applied voltage for several temperatures for 0.2 at% Ni-doped SrTiO$_3$. Experimental result (symbols) and the low field and medium field simulation (lines) obtained by Eq. (15) are plotted together. The fitting parameter was the diffusion constant of the holes taken from Ref. [24], the barrier height $\Phi_{GB}(T)$ and the Fermi level both obtained from the defect chemical simulation (Ref. [1]). The critical field strength E_{crit} is obviously temperature independent and is about $2 \cdot 10^7\,$V/m for the average GB field stress. For the simulation of the temperature dependence of the barrier $\Phi_{GB}(T)$, a slight temperature dependence of the Fermi level is included. Figure 7 shows the plot of σ_{GB} vs. the temperature together with the simulated one by Eq. (15) at low voltages $V = 1\,$V and a Fermi level of 0.9–1.1 eV.
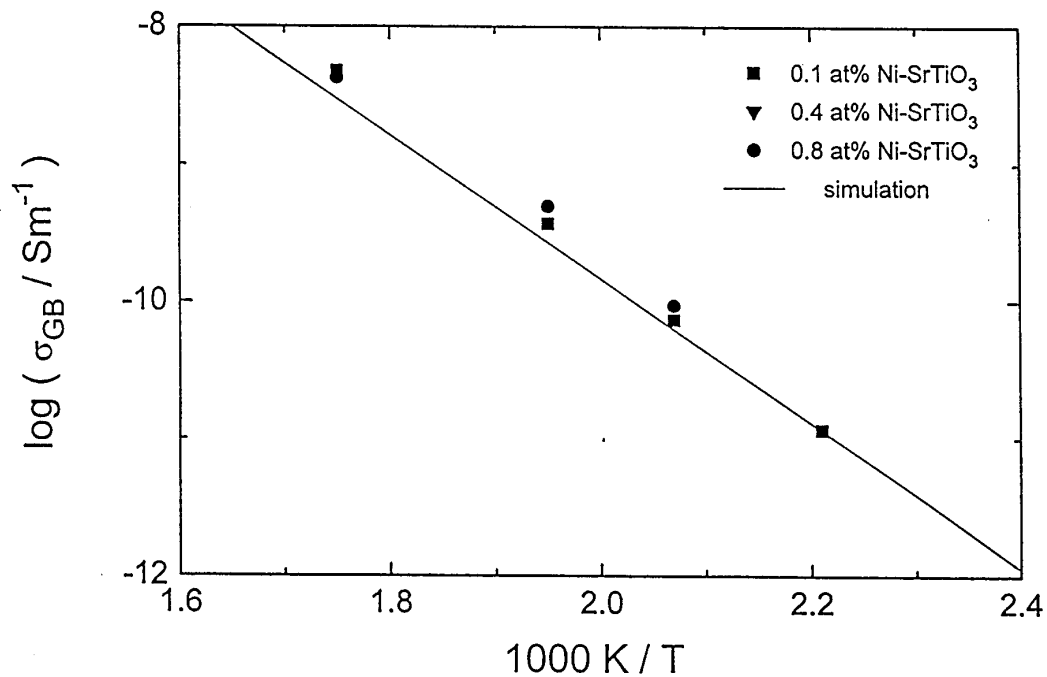
Fig. 7. Temperature dependence of the low field σ_{GB} ($\bullet$, $\blacksquare$) in the temperature range of the V-profile obtained by measurement together with the numerical result obtained from Eq. (14) for $U = 1$ V (solid line).
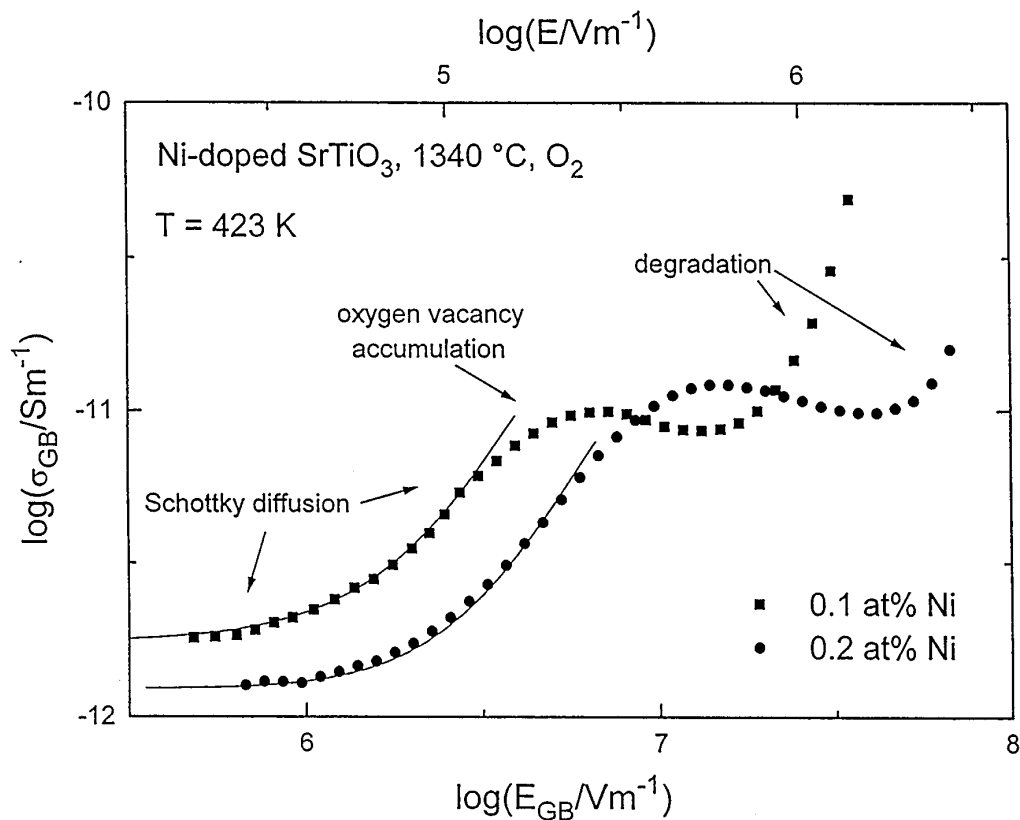

Fig. 8. Field dependence (external applied field $E = V/D$, where D denotes the overall sample thickness) of the GB-conductivity σ_{GB} for (a) 0.1 at% Ni-doped SrTiO$_3$ ($\bullet$) and (b) 0.2 at% Ni-doped SrTiO$_d$ ($\blacksquare$) at $T = 423$ K and $t = 300$ s. Solid curves: numerical results obtained from Eq. (14). Above $E_{GB} = 10^7$ V/m: interference with resistance degradation.

The activation energy of the semi-saturation plateau at higher fields (Fig. 3) is the same as the low field GB conductivity ($\cong 1$ eV) which is in accordance with Eq. (15) and is dominated by the height of the Fermi level. Changing the barrier height has no influence on the Fermi level ΔW_F within the bulk, which defines Schottky diffusion over the barrier.

(5) Effect of Acceptor Concentration

Figure 8 shows the field dependence of the GB conductivity for different acceptor concentrations. In Eq. (16) the low-field GB conductivity is slightly dependent on the acceptor concentration which is in agreement with our recent paper [1]. Combining Eqs. (16) and (17) one obtains a square root dependence of the GB conductivity on the acceptor concentration and the simulation fits well with the measurements.

When comparing ceramics with different acceptor concentrations, one has to keep in mind their different grain sizes leading to different critical field stresses E_{crit}. For ceramics with large grains (0.4 at% Ni: 23 μm, 0.8 at% Ni: 11 μm), the field stress at the grain-boundaries is 1 order of magnitude higher than in small grain size ceramics (0.1 at% Ni: 2.3 μm, 0.2 at% Ni: 2.7 μm) in accordance with Eq. (8). Hence E_{crit} for the large grain samples is one order of magnitude lower in comparison to the small ones.

V. Conclusions

Using Ni-doped SrTiO$_3$ as a model system for acceptor-doped perovskite structured ceramics, the field enhanced GB conductivity σ_{GB} revealed by impedance spectroscopy in the time domain was investigated and the effect of temperature and acceptor concentration on the *high field* σ_{GB} were investigated. Based on the data presented in this paper, we conclude the following:

(1) The GB potential barrier is reduced, but does not completely vanish after applying high fields.

(2) The field enhanced conductivity is predominately electronic due to holes and can be explained in terms of a Schottky diffusion model in the case of V-shaped carrier concentration profiles at the grain boundaries.

(3) The experimental temperature dependence of the low-field GB conductivity is in good accordance with Schottky diffusion theory and is determined by the Fermi level ΔW_F within the bulk.

(4) The high field, saturated GB conductivity shows the same activation energy as the low field GB conductivity.

(5) The slight decrease of the GB conductivity after reaching the saturation point can be described qualitatively by an accumulation of oxygen vacancies, which is a precursor for the resistance degradation.

(6) The dependence of the field enhanced GB conductivity σ_{GB} on the acceptor concentration is in good accordance with values obtained by the Schottky simulation.

(7) Schottky diffusion can quantitatively explain the low field and the field enhanced regime of the GB conductivity.

(8) The positive interface charge $Q_{GB}^{\square}$ is not voltage dependent for low and medium field stresses.

Acknowledgment

References

1. M. Vollmann, R. Hagenbeck, and R. Waser, *J. Am. Ceram. Soc.*, to be published.
2. M. Vollmann and R. Waser, *J. Am. Ceram. Soc.*, **77**[1], 235–243 (1994).
3. Ch. Tragut and K.H. Härdtl, *Sensors and Actuators*, **B4**, 425–430 (1991).
4. T. Bieger, J. Maier, and R. Waser, *Sensors and Actuators*, **B7**, 763–768 (1992).
5. R. Waser, *J. Am. Ceram. Soc.*, **74**[8], 1934–1940 (1991).
6. R. Waser, T. Baiatu, and K.-H. Härdtl, *J. Am. Ceram. Soc.*, **73**[6], 1645–53 (1990).
7. R. Waser and M. Klee, *Integrated Ferroelectrics*, **2**, 23–40 (1992).
8. R. Waser and D. Smyth, in edited by C.P. de Araujo, J.F. Scott, and G.W. Taylor, pp. 47–92, Gordon and Breach USA (1996).
9. H. Neumann and G. Arlt, *Ferroelectrics*, **69**, 179–186 (1986).
10. Sze, 2nd edition, John Wiley & Sons N.Y., 1981.
11. O'Dwyer, Clarendon Press, Oxford, 1973.
12. Atkins, 3rd edition, Oxford University Press, 1987.

13. F. Greuter, G. Blatter, M. Rossinelli, and F. Stucki, *Adv. Varistor Technol., Ceram. Trans.*, **3**, 31–53 (1989).
14. G.E. Pike, *Mater Res. Soc. Proc.*, **5**, 369–379 (1982).
15. G.E. Pike, *J. Appl. Phys.*, **50**[5], 3414–3422 (1979).
16. H. Ihrig, *J. Phys. C: Solid State Phys.*, **9**, 3469–3474 (1976).
17. H. Böttger and V.V. Bryskin, p. 45 VCH (1985) Weinheim.
18. Ch. Weißmantel and C. Hamann, p. 598, Springer-Verlag (1980) Heidelberg.
19. R. Hagenbeck, private communications (to be published).
20. W. Schottky, *Naturwissenschaften*, **26**, 843 (1938).
21. R. Waser, edited by N. Setter and E.L. Colla, p. 213, Birkhäuser Verlag (1993) Basel.
22. N.F. Mott, p. 231, Taylor & Francis LTD London, (1974).
23. Y.-M. Chiang and T. Takagi, *J. Am. Ceram. Soc.*, **73**[110], 3278–3285 (1990).
24. J. Maier, *J. Am. Ceram. Soc.*, **76**[5], 1223–1227 (1993).
25. I. Denk, W. Münch, and J. Maier, *J. Am. Ceram. Soc.*, **78**[12], 3265–3272 (1995).
26. H.J. Hagemann and D. Hennings, *J. Am. Ceram. Soc.*, **64**[10], 590–594 (1981).
27. M. Vollmann, in Ger. Ph.D.-thesis, *Fortschrittsberichte VDI-Reihe 5*, VDI-Verlag Düsseldorf, (1997).